Planetary equatorial trapped waves in the Atlantic ocean from TOPEX/POSEIDON altimetry

Carlos França [*] [a], Ilana Wainer [a], Afranio R. de Mesquita [a] and Gustavo Goni [b]

[a]Department of Physical Oceanography of the University of São Paulo, Brazil

[b]NOAA/Atlantic Oceanographic and Meteorological Laboratory, Miami, Florida

Planetary equatorial waves are important mechanisms for the adjustment of the tropical oceans. The identification and role of planetary equatorial waves in the tropical Atlantic is investigated by taking advantage of unprecedented accuracy, coverage and resolution of the TOPEX/POSEIDON altimeter data, from 1992 to 1999. This is accomplished by projecting the sea level height anomalies, obtained from the altimetry for the tropical Atlantic basin onto the linear equatorial meridional waves, first baroclinic mode. Results presented here show the existence of equatorial Kelvin and Rossby modes, as well as their significant reflection off the African coast.

1. INTRODUCTION

The mean ocean dynamics in the tropical Atlantic is characterized by a meridional heat transport from south to north [*Hastenrath*, 1982], which is a part of the *Global Conveyor Belt* [*Gordon*, 1986]. Estimates of this interhemispheric transport are particularly difficult at equatorial latitudes due to a complex system of zonal currents and counter-currents that present temporal scales of variability that range from daily to interannual. The surface parameters, such as sea height and sea surface temperature, are linked to the upper ocean ocean dynamics and its variability, and to steric-related effects in the upper hundreds of meters. The separation of these signals into each of its different components is key to the understanding of the surface circulation. In this work we investigate in some detail the surface height and temperature signals associated with the equatorial wave dynamics and to clarify the nature of this variability at interannual time scales in the tropical Atlantic.

One of the most important characteristic of the tropical oceans is its ability to support fast zonally propagating movements. The most typical example of these movements are the equatorially trapped waves that were first theoretically described by *Matsuno* [1966]. These waves, which are efficient carriers of informa-

[*]Corresponding author address: Carlos A. S. França, Universidade de São Paulo, Department of Physical Oceanography, Praça do Oceanográfico 191, São Paulo, SP 05508-900 - Brazil, phone: (55–11)–3091 6564, Internet: cafranca@usp.br

tion along the equator, can lead to remote effects. For example, a wind event (westerly or easterly) can excite Rossby waves that propagate westwards, reflecting off the western boundary as Yanai and Kelvin waves or can also excite Kelvin waves which propagate eastward, reflecting off the eastern boundary as Rossby waves and coastal Kelvin waves [*Moore and Philander*, 1976]. The linear response of the upper ocean can be interpreted as a complex superposition of these waves. A critical point is to establish methodologies to identify these processes of wave dynamics through data obtained from suitable measurements.

The relation between planetary equatorial waves and the El Niño Southern Oscillation (ENSO) phenomenon in the Pacific ocean was early suggested from sea height data obtained on islands [*Wyrtki*, 1975]. The *delayed oscillator* theory [*Schopf and Suarez*, 1988; *Battisti*, 1988] proposes a central role for long equatorial waves and its reflection on the western Pacific for a El Niño cycle. Observations of such mechanisms are difficult using *in situ* methods. First attempts to fit meridional equatorial wave modes to altimetry measurements took place in the Pacific ocean to investigate the ENSO phenomenon [*Delcroix et al.*, 1991, 1994]. More recently, and within the same context, TOPEX/POSEIDON (T/P) data were examined to test the *delayed oscillator* theory [*Boulanger and Menkes*, 1995; *Boulanger and Fu*, 1996; *Boulanger and Menkes*, 1999]. One interesting aspect of these studies is that they did not reveal important equatorial wave reflection in the western Pacific. However, they strongly suggested their reflection in the east, off the South American coast, leading to a modification of the *delayed oscillator* theory [*Picaut et al.*, 1997]. Furthermore, using T/P data, *Delcroix et al.* [2000] found that western reflection of equatorial waves contribute marginally to the onset of El Niño and La Niña events from 1993 to 1998.

Unlike the tropical Pacific, where interannual variability is dominated by the ENSO phenomenon, multiple competing influences of comparable importance affect the tropical Atlantic. Anomalies in the tropical Atlantic sea surface temperature (SST) are primarily driven by changes in surface fluxes, which can be forced either locally or remotely – an example of local forcing arises from changes in the position and intensity of the (wind driven) Inter-Tropical Convergence Zone (ITCZ), while remote forcing could come from variability over the extra-tropical Atlantic or from ENSO [e.g., *Servain et al.*, 1998]. The seasonal cycle in the tropical Atlantic is the surface signal with the largest atmosphere-ocean amplitude [*Merle*, 1980a; *Merle et al.*, 1980]. However, interannual and longer-term variations are not negligible and, at least in part, can be interpreted as modulations to the average annual cycle [*Servain et al.*, 1998]. In the tropical Atlantic, two modes of coupled atmosphere-ocean variability superimposed on the mean seasonal cycle can be identified [*Servain and Merle*, 1993]. The first mode is characterized by a north-south interhemispheric gradient in SST with associated changes in trade winds that exerts considerable influence on the regional climate [*Moura and Shukla*, 1981; *Servain*, 1991]. This mode has no Pacific counterpart and it features anomalies on either side of the ITCZ, and has time scale ranging from interannual to decadal [*Servain*, 1991]. The well known droughts in Northeast Brazil and in sub-Sahara Africa are often found to be associated not only with the anomalously

warm or cold SST anomalies in the tropical north-south Atlantic, but also with the north-south migrations of the ITCZ [*Moura and Shukla*, 1981]. The second mode is an equatorial mode of variability similar to ENSO [*Hisard*, 1980; *Merle*, 1980b; *Shannon et al.*, 1986; *Zebiak*, 1993; *Carton and Huang*, 1994]. This equatorial mode has time scales that range from 2 to 4 years and it is similar to, albeit much weaker than, the Pacific ENSO as it relates changes in the tropical ocean thermal structure to trade wind anomalies in the western Atlantic [*Servain*, 1991; *Zebiak*, 1993]. Specifically, when trade winds intensify (weaken), the equatorial thermocline slope increases (decrease), and negative (positive) SST anomalies develop in the eastern equatorial ocean, particularly in the Gulf of Guinea. These equatorial SST anomalies have been shown to have an effect on rainfall in the Gulf of Guinea region [*Wagner and da Silva*, 1994].

Although the atmosphere-ocean coupling is evident for these two modes [*Moura and Shukla*, 1981; *Wagner and da Silva*, 1994], the mechanisms responsible for them are not clear. The planetary free waves are expected as part of the ocean dynamics response of the Atlantic remote forcing. Although equatorial waves and their seasonal time scales have been investigated using GEOSAT altimetry observations [*Arnault et al.*, 1992; *Arnault and Cheney*, 1994; *Gourdeau et al.*, 1997], their interannual times scales still need to be established. Kelvin waves were observed in studies using dynamical heights derived from inverted echo sounders [*Katz*, 1987] and T/P-derived sea heights [*Katz*, 1997] for intra-seasonal scales in the Atlantic Ocean. These waves are present and important in numerical models of the tropical Atlantic only when linear dynamics are considered [*Busalacchi and Picaut*, 1983; *McCreary et al.*, 1984; *duPenhoat and Gouriou*, 1987]. However, its role in General Circulation Models (GCMs) [*Philander and Pakanowski*, 1986; *Schott and Boning*, 1991] is not as evident.

The objective of this work is to use the sea height data and, taking advantage of its unprecedented accuracy, coverage and resolution of the TOPEX/POSEIDON (T/P) measurements, to investigate the presence of the planetary equatorial waves in the tropical Atlantic and its relationship to the Equatorial mode from 1992 to 1999. The sea height and sea surface temperature data, their processing and preliminary results on equatorial propagating signals at the equatorial Atlantic are presented in section 2. The equatorially trapped modes are reviewed in section 3 in order to explain the framework of modes and the modal decomposition of the sea level and sea surface temperature anomalies. Results of data projection onto equatorial waves in the tropical Atlantic, its variability and correlation characteristics among the modes are presented in section 4 and discussed in section 5. Results are summarized and concluded in section 6.

2. SEA HEIGHT AND SEA SURFACE TEMPERATURE DATA

The T/P-derived sea height data was obtained from the Merged Geophysical Data Records version C (MGDR-C) distributed by the Centre National d'Etudes Spatiales (CNES) Arquivage, Validation et Interprétation des données des Satellites Océanographique (AVISO) system [*AVISO*, 1996]. This data is analyzed for the

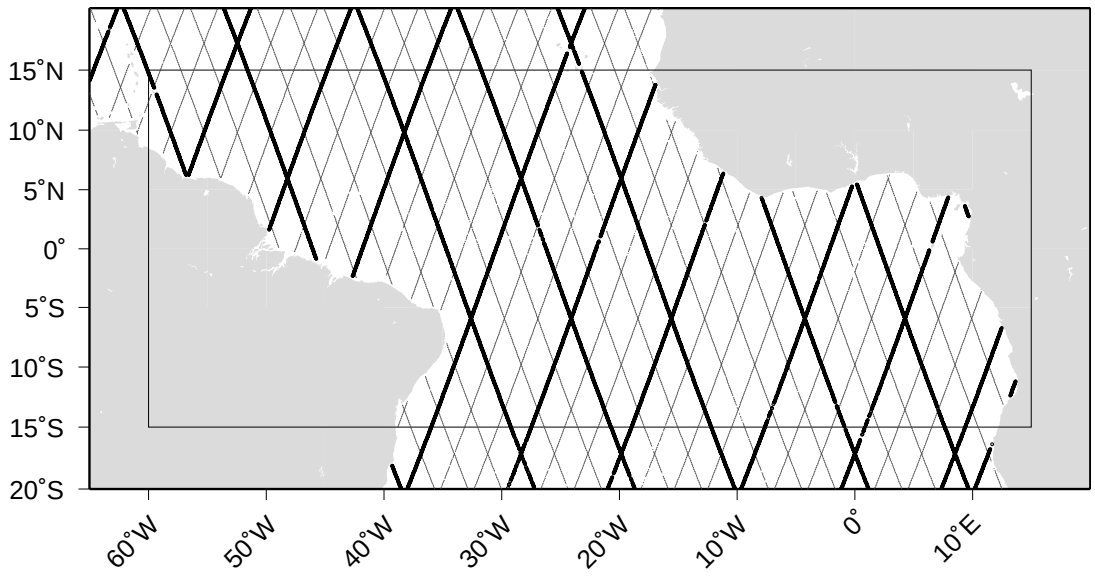

Figure 1. The region of study. The T/P groundtracks are superimposed. Tracks occurring in the first third period (3.3 days) of the cycle are shown with a thicker line.

period going from October 1992 to May 1999, corresponding to cycles 001 through 244. The region of study is located in the tropical Atlantic ocean and bounded by 15°N - 15°S and 60°W - 20°E (Figure 1).

Corrections due to electromagnetic signal propagation and surface interaction were applied. Modeled manifestation in the sea level of Solid Earth Tide [*Cartwright and Tayler*, 1971], Pole Tide [*Wahr*, 1985], Dry tropospheric and Inverted Barometer [ECMWF model, *AVISO*, 1996] were removed. Elastic Ocean Tide was also removed using a filtering procedure that can be used over shallow shelf areas [*França et al.*, 2001].

The alongtrack T/P measurements were re-sampled every 1/3° in latitude by fitting a second-degree polynomial locally to the data within a 1/6° radius to create equally spaced data and to smooth out small wavelength noise. Sea height anomalies (SHA) were computed by subtracting the 4 year (1993-1996) mean to remove the Geoid uncertainties. The SHA were mapped onto a regular $1^\circ \times 1^\circ$ (latitude$\times$longitude) grid at 10.14 days time intervals, and its uncertainty estimated using an Optimal Linear Interpolation (OLI) method [*Liebelt*, 1967]. Decorrelation scales of 150 km for every position (r_i) within the region and 15 days for every time (t_j) within the period were estimated by analyzing the correlation function obtained by inverting mean spectra estimation, using the Wold theorem [*Priestley*, 1981], for the region of study and during the period 1992 to 1999. Only observations encompassed by a window centered at the point $(\vec{r_i}, t_j)$ with 4° diameter and 30 days time interval were considered for interpolation. Within 100 km of the coasts, the uncertainty of SHA estimated by the OLI is usually less than 5

cm although it can reach up to 10 cm particularly at some areas, such as in the Amazon river mouth. This uncertainty is of order of 2 cm far from continental boundaries, slightly smaller along T/P tracks, but increasing towards the center of the diamond shaped areas formed by adjacent crossing altimeter groundtracks. This uncertainty, with variance of the order of 4 cm^2, remains almost unchanged when larger decorrelation scales, ranging from 500 to 1000 km and eventually anisotropic, are used in the OLI, when the small scale diamond shaped variability disappears causing the sea height maps to be smoothed.

The tropical Atlantic ocean has variability dominated by the forced seasonal cycle [*Merle*, 1980a; *Merle et al.*, 1980], which is not the main interest of this work. Equatorial waves are best identified using the sea height residues, which are the sea height anomalies with the annual-cycle removed (SHAA). The SHA data was deseasoned by removing the mean seasonal cycle estimated from 4 years of altimetric observations, during the period 1993 to 1996. These SHAA fields are partly related to the ocean thermal energy anomalies [*Gill and Niiler*, 1973; *Chambers et al.*, 1997]. Weekly sea surface temperature anomalies (SSTA) were obtained by referring the SST values to the seasonal climatology from the IGOSS-NMC (Integrated Global Ocean Services System Products Bulletin-National Meteorological Center) data set [*Reynolds and Smith*, 1994] for the period October 1992 to May 1999, corresponding to T/P cycles 001 through 244.

Space-time (longitude vs. time) diagrams of SHAA and SSTA at the equator are shown in Figure 2, showing the expected consistency in the equatorial Atlantic. The correspondence between SHAA and SSTA is more evident in the central, around 20°W, and western, around 40°W, basins in the equatorial Atlantic, than in the eastern basin, around 0° (Greenwich Meridian). For example, during 1997, cold SST anomalies associated with negative SHAA in the central basin become warmer east of 20°W associated with the increase of negative SHAA. The same pattern but with opposite phase (warm SSTA and positive SHAA) occurs in 1998 during an Atlantic *Warm Event* [e.g., *Servain et al.*, 1999]. Eastward propagation of anomalies is observed in the SHAA data (Figure 2, left panel) but not in the SSTA (Figure 2, right panel).

The zonal propagation velocity at the equator can be estimated directly from the space-time diagrams or in a slightly more rigorous manner by inspecting the lagged correlation as a function of longitudinal separation. At 20°W, these correlations are presented at the equator in the SHAA (Figure 3, left) and SSTA (Figure 3, right) fields. The confidence level of 95% is approximately reached for correlations above 0.3 and the 99% above 0.4 (gray shades in Figure 3), as obtained from 50 independent estimates of the variable. Significant correlation for positive (negative) lags east (west) of a given longitude shows that the variable appears first (later) east and later (first) in the western (eastern) section of the basin, evidence of a westward (eastward) propagation.

The zonal velocity of 1.7 m/s eastward and -0.57 m/s westward can be obtained from the lag vs. longitude correlations (slanted lines in Figure 3). The most significant correlations are aligned with the 1.7 m/s eastward propagation line with some indication of westward propagation along the -0.57 m/s line. The zonal propaga-

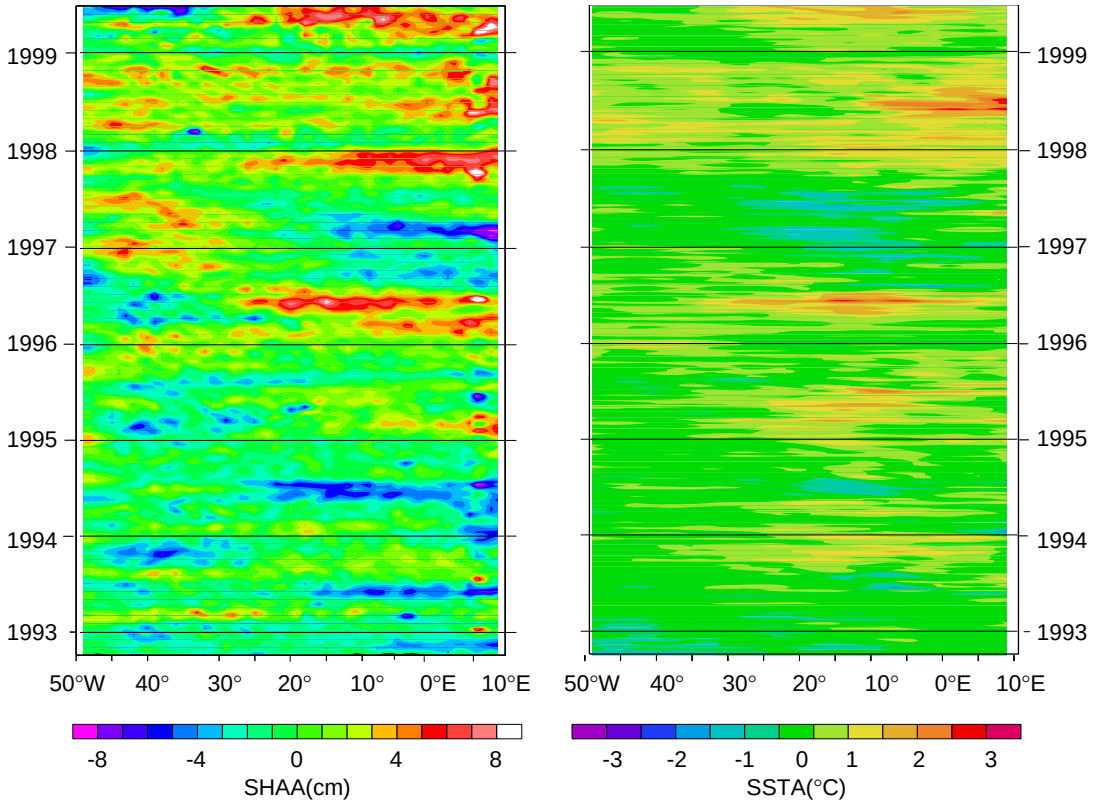

Figure 2. Time × Longitude diagram for (left) T/P SHAA and (right) SSTA at the equator in the Atlantic ocean for the period October 1992 to May 1999.

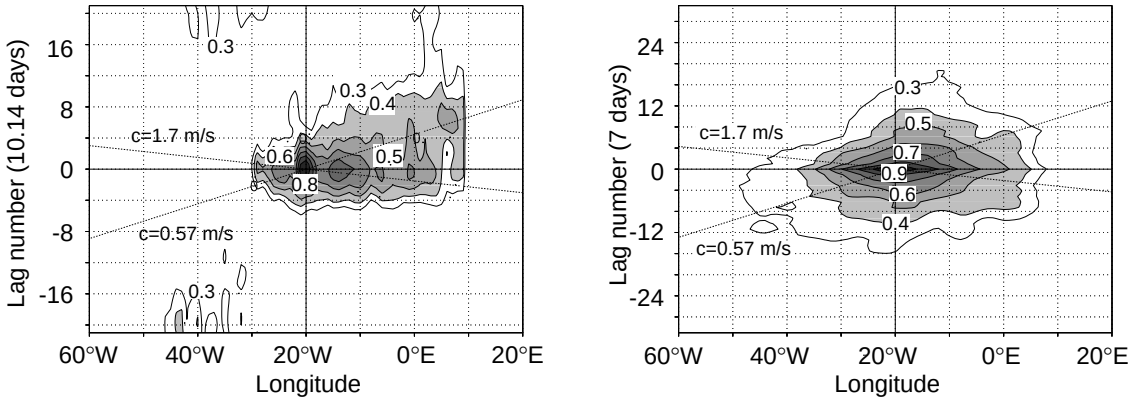

Figure 3. Lag vs. Longitude correlation at the equator, 20^{o}W, for (left) SHAA and (right) SSTA. Correlation significant at the 95% (99%) confidence limit is contoured (shaded).

tion is not evident in the SSTA field. Moreover, examination of several other lag vs. longitude correlation plots at different longitudes (not shown) reveal the same lack of propagation of SSTA, while the dominant signal in the SHAA field is estimated to be 1.7 $\pm$ 0.2 m/s. These results indicate a partial lack of correspondence between these two parameters, which can be explained because the sea height is an integral of the thermal and dynamical effects of the ocean upper layers and may not always be correlated with the sea surface temperature anomalies, particularly at equatorial latitudes [*Knudsen and Andersen*, 1997; *Mayer et al.*, 2001, Mayer *et al.*, this volume].

3. EQUATORIALLY TRAPPED MODES

The sampling of the ocean by altimetry, and specifically by T/P in our study, limits the observation of equatorial waves. Due to the satellite 10-days repeat cycle, the fast inertia-gravity waves with periods shorter than 20 days cannot be observed. Although the alongtrack resolution of SHA used here is of about only 7 km, the separation of adjacent groundtracks is of 315 km in equatorial latitudes (the effective separation is somewhat smaller due to the diamond areas formed by T/P groundtracks) not allowing observation of waves smaller than 200 km, zonally at the equator. The meridional dependence of the waves at the equator is sampled at the alongtrack resolution. For small wavenumber motions, with wavelengths larger than 1000 km, the time resolution of the T/P data is of order of 3 days, if a sub-cycle period of the satellite is considered (Figure 1).

In order to characterize equatorial trapped waves their zonal dispersion relationship is shown in Figure 4 (left panel) for the first baroclinic mode, c=1.7 m/s, [*Matsuno*, 1966] for periods longer than 1 day and zonal wavelength larger than 200 km. The upper branches, which are symmetric to their wavenumber, show eastward (positive wavenumber) and westward (negative wavenumber) phase velocities, are the inertia-gravity modes. The lower branches, negative wavenumber (westward phase velocity) are the equatorially trapped Rossby modes; the positive wavenumber linear branch is the non-dispersive equatorial Kelvin wave; and the branch with negative wavenumber and lower frequencies and positive wavenumber for higher frequencies is the mixed Rossby-gravity or Yanai wave [*Matsuno*, 1966]. The horizontal line in this same figure shows the Nyquist frequency (20 days period) for the T/P sampling. Figure 4 (right panel) shows the same dispersion relation but for the wavenumber-frequency domain that can be observed by this altimeter where only planetary Rossby and Kelvin equatorial modes are in the domain observed by T/P altimetry.

The meridional dependence of the planetary equatorially trapped waves is given by Hermite functions, which are orthogonal over an infinite domain. However, they can also be considered approximately orthogonal over a sufficient large finite interval. Figure 5 shows the meridional dependence of the amplitude of the Kelvin and first five Rossby equatorial waves, first baroclinic mode (c=1.7 m/s), between 15°N and 15°S. It can be seen that the amplitudes of all of these meridional modes are nearly zero for latitudes higher than 10°N and lower than 10°S. The sea height

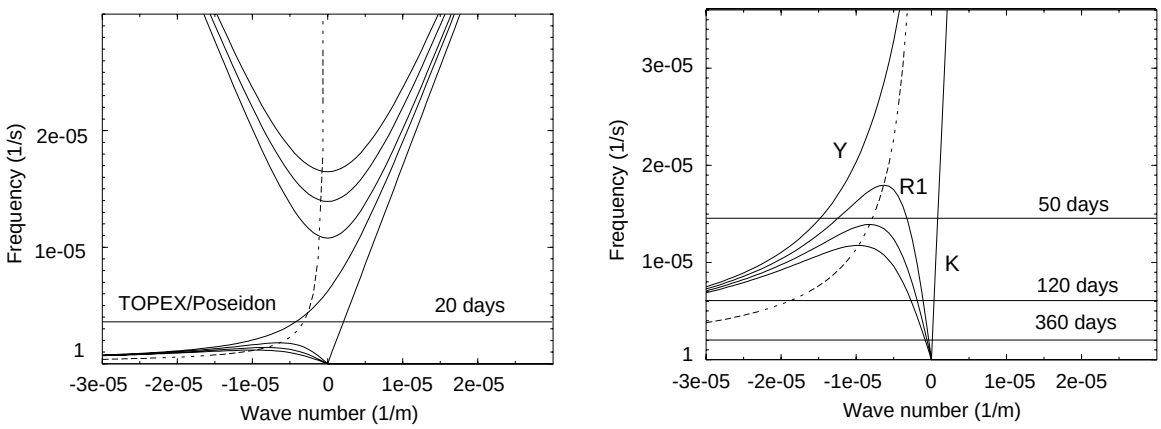

Figure 4. Dispersion relationship for the first baroclinic mode (c=1.7m/s) of the long equatorial trapped waves [adapted from *Matsuno,* 1966]. (left) Frequency-wavenumber domain of the solution and (right) frequency-wavenumber domain seen by T/P sampling with the branches for Yanai, Rossby first meridional mode and Kelvin waves labeled by Y, R1 and K, respectively.

anomaly, η can be written as a sum of meridional modes, given by Hermite functions, H_i, multiplied by weights or wave coefficients, h_i, which are functions of time and longitude:

$$\eta(x, y, t) = \sum_{i=1}^{\infty} h_i(x, t) H_i(y). \tag{1}$$

A finite N-dimensional subspace can be considered as an approximation of (1) by choosing the dominant modes:

$$\eta(x, y, t) = \sum_{i=1}^{N} h_i(x, t) H_i(y). \tag{2}$$

Assuming that the sea surface temperature has the same meridional dependence as the sea height, the Kelvin wave and the first 14 Rossby meridional modes are used as a vectorial basis onto which the mapped T/P altimeter and SST data are projected in the least square sense. Effectively, it is a finite Fourier-Hermite transform by which the coefficients, or wave amplitudes h_i, are estimated for each time and longitude. Only longitudes where an equatorial belt of 4° latitude have observational data over the ocean are considered, which in the region of study is an area bounded by longitudes between 44°W and 10°E.

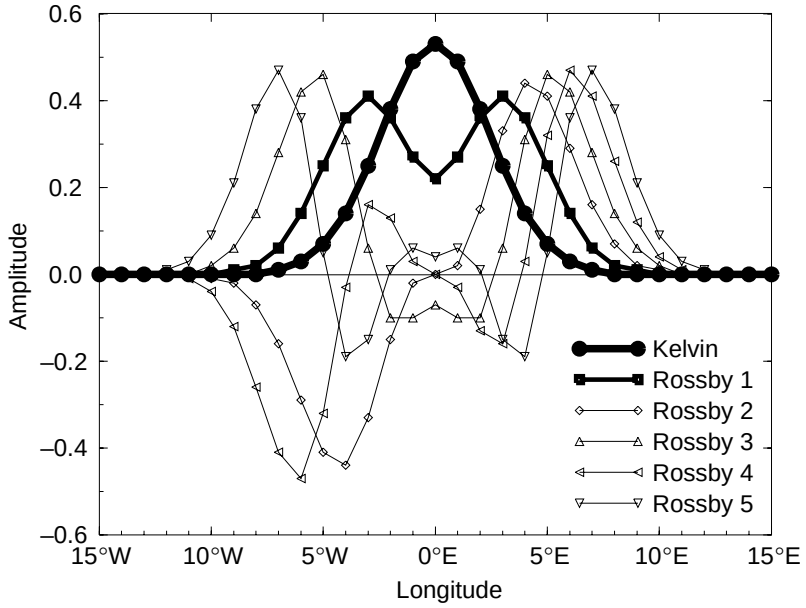

Figure 5. Normalized amplitude of the lowest 5 meridional modes of the planetary equatorially trapped waves, for the first baroclinic mode (c=1.7m/s).

4. RESULTS

The projection of mapped data over the space spanned by the first 15 baroclinic meridional equatorial wave modes (N=15 in (2)) results in the wave coefficients, h, related to wave amplitudes in units of length or temperature, as functions of longitude and time. Most of the SHAA and SSTA variance of these coefficients (Figure 6, left and right panels respectively) is contained in the first 3 meridional modes, mainly the first two: Kelvin and Rossby-1 waves. The variance increases and more meridional modes show enhanced relative contribution near the South American and African coasts. The percentage of the SHAA variance captured by each zonally averaged mode is shown for the total north-south extent considered (15°N-15°S) and for an equatorial band (5°N-5°N) in Figure 6, for SHAA and SSTA, to address the relative importance of these waves at closer equatorial latitudes. The first meridional Rossby wave mode appears to be the most important, capturing between 20% of the total SHAA variance explained (Figure 6, left), and 30% of the total SSTA variance explained (Figure 6, right). The variance explained varies between 40% and 60% when only the equatorial band is considered.

Considering 10% of the sea height variance explained as the threshold for wave detection, only the Kelvin and the first Rossby modes are present when the entire region (15°N - 15°S) is considered, both in SHAA and SSTA data. When only the equatorial band (5°N - 5°S) is considered, Rossby-1 and Kelvin modes explains 80% and 85% of the total variance of the SHAA and SSTA data. However, the variance contained in the 15 modes is slightly higher than the variance contained in the original data, as the integral of these spectral estimates is larger than 100%, when the

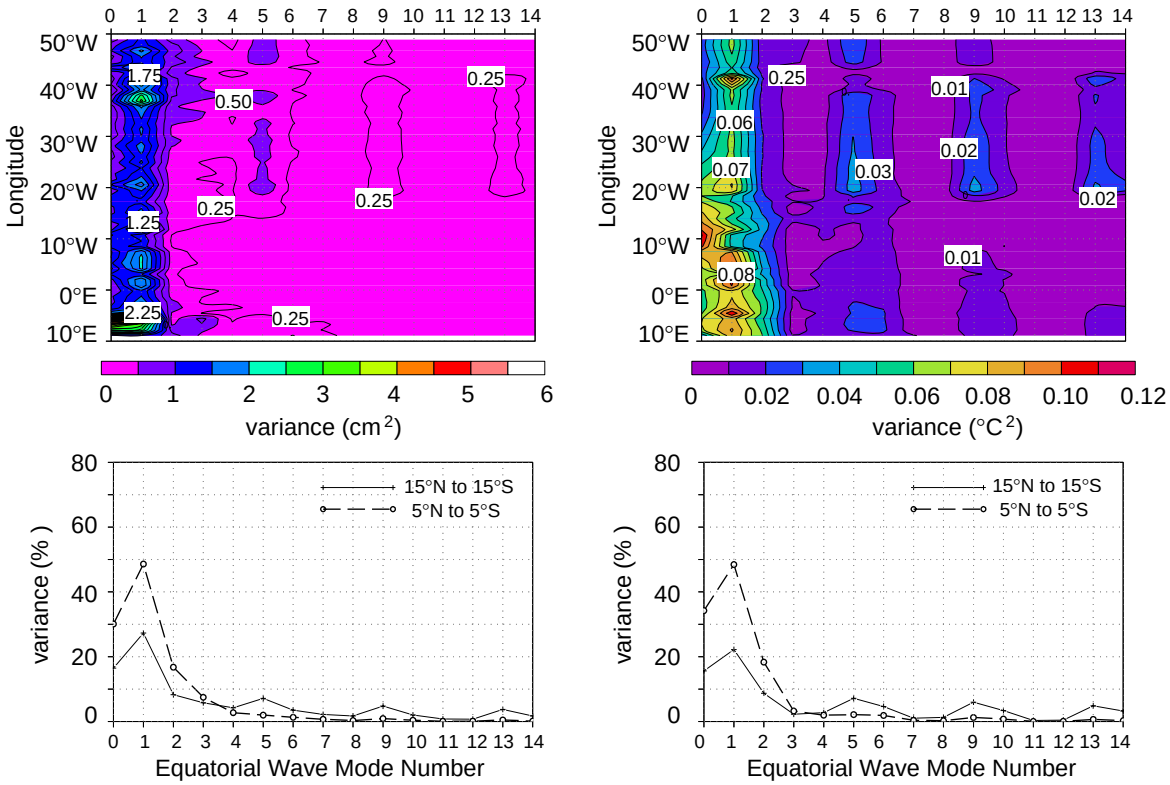

Figure 6. Variance explained by the meridionally trapped equatorial modes (Kelvin and the lowest 14 Rossby modes) for the October 1992 to May 1999 period for (left) T/P SHAA and (right) observed SSTA. Upper panel - meridional averages as function of longitude. Lower panel - meridional and zonal averages.

analysis is limited to the equatorial belt, and probably due to the non-orthogonality of the modes over the finite meridional domain. This non-orthogonality can also be responsible for the small side lobes observed at modes 5, 9 and 13 but non-optimal choice of the modal structure could also show this effect.

Space-time diagrams of the SHAA and SSTA wave coefficients, h, of the Kelvin, Rossby-1 and Rossby-2 are shown in Figure 7a and 7b, respectively. The numerical values of these coefficients are approximately twice the wave amplitude in centimeters or degrees. Uncertainty in the coefficients of SHAA are of order of 0.5 cm (1 wave coefficient units in Figure 7a), assuming white noise variance of 4 cm^2 equally distributed among the 15 modes considered. The uncertainty in the wave coefficient of SSTA (Figure 7b) is 0.4 °C (or 0.2 wave coefficient units), assuming standard error of 0.4 °C in the tropical Atlantic [*Reynolds and Smith*, 1994].

Positive (negative) coefficients of SHAA represent values of sea height above (below) the mean sea height, which are characteristic of the downwelling (upwelling) produced by meridionally symmetric waves – Kelvin and Rossby-1. On the other hand, for Rossby-2 (which is antisymmetric with respect to the equator), a positive coefficient corresponds to downwelling to the north and upwelling to the south of

(a)

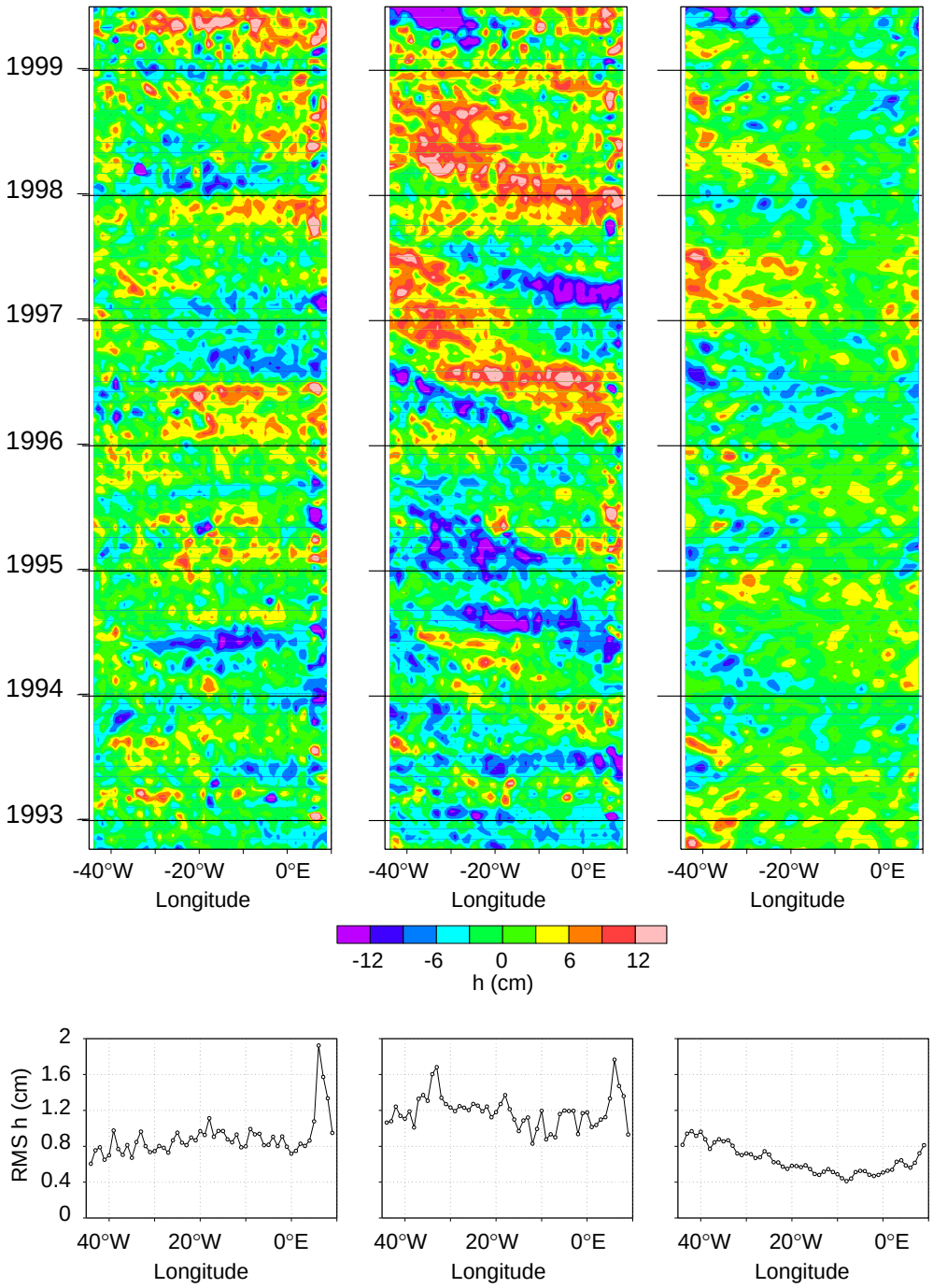
1999
1998
1997
1996
1995
1994
1993
-40°W
-20°W
0°E
Longitude
-12
-6
0
6
12
h (cm)
RMS h (cm)
2
1.6
1.2
0.8
0.4
0

(b)

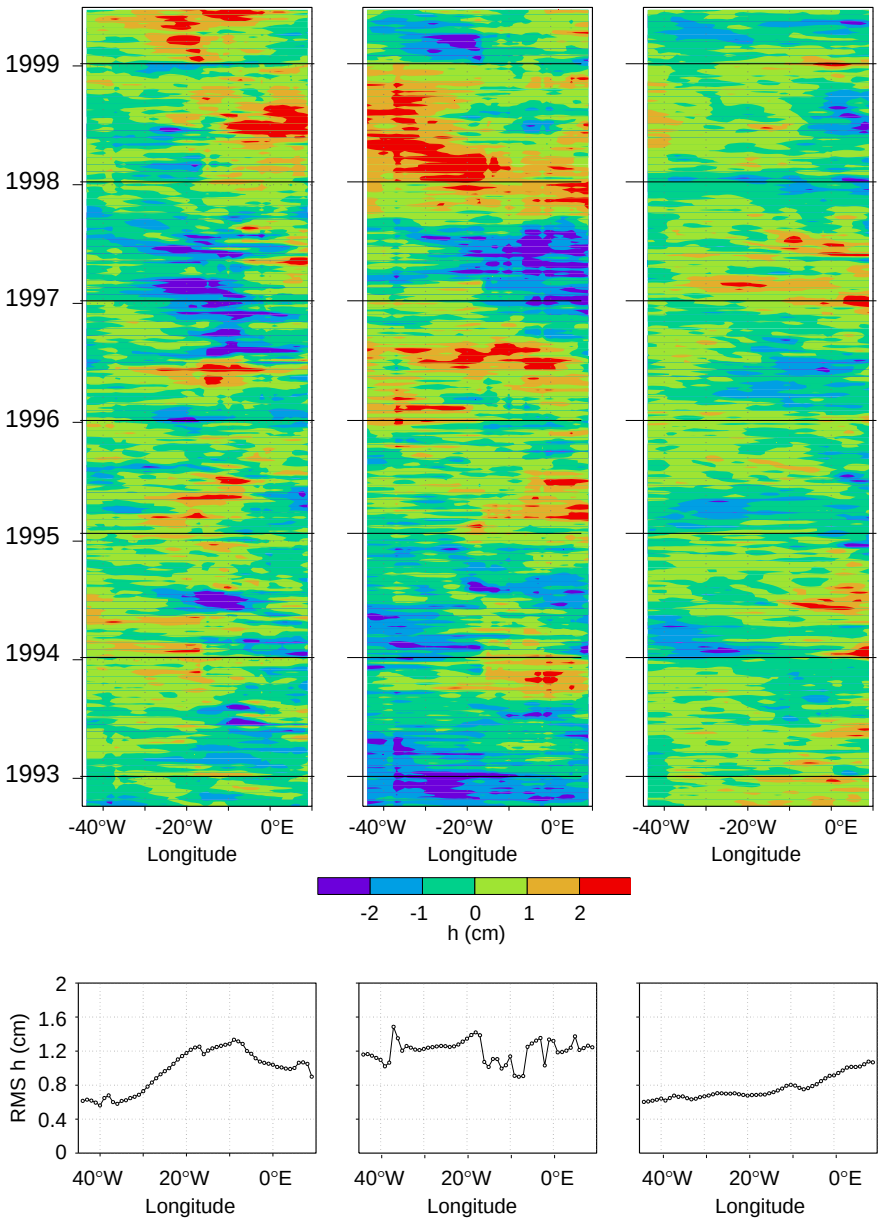

Figure 7. Time-Longitude diagram for the wave coefficient h of the (left) Kelvin wave, (center) Rossby-1 and (right) Rossby-2 waves, first baroclinic mode (c=1.7m/s) from (a) T/P SHAA and (b) observed SSTA. Lower panels show the Root Mean Square (RMS) of the wave coefficient, h, for the period.

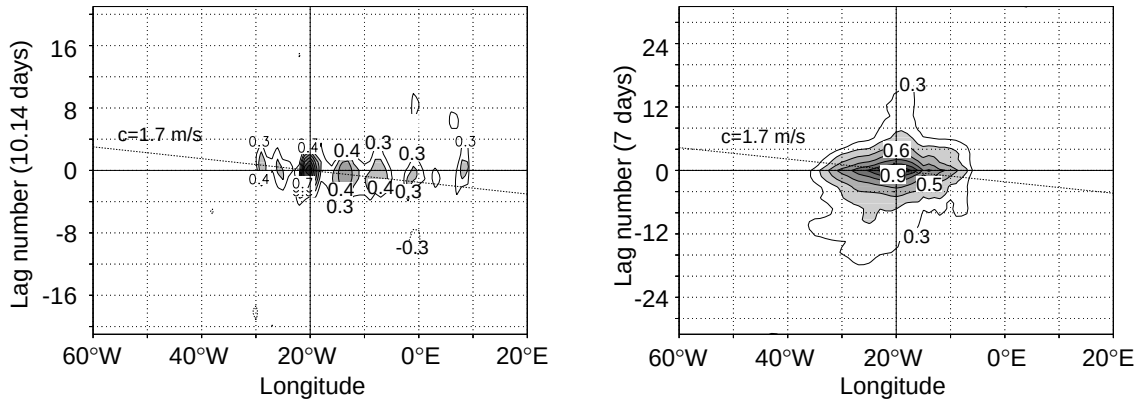

Figure 8. Lag vs. Longitude Correlation at 20^oW, for the Kelvin wave coefficient for (left) SHAA and (right) SSTA. Correlation significant at the 95% (99%) confidence limit is contoured (shaded).

the equator. For the SSTA, positive (negative) values are associated with warmer (colder) surface waters. The fast eastward propagation is evident in the Kelvin wave coefficients for SHAA (Figure 7a) but not as clear for SSTA, due to the higher frequency variability (which does not show propagation) and lack of east-west coherence of the anomalies (Figure 7b). Figure 8 presents the lag vs. longitude correlation of the Kelvin wave coefficients at 20°W for SHAA (left panel) and SSTA (right panel). The phase velocity of the SHAA is estimated from the diagrams and ranges between 1.2 to 1.6 m/s. Propagation characteristics for the Kelvin wave coefficient of SSTA are not evident.

Examination of SHAA shows that the Kelvin mode is dominated by intra-annual events with 2 to 4 years time scale and 2 to 3 cm amplitude. Interannual variability can also be observed. The interannual variability at the 2 to 4 year time scale is observed mainly at the central part of the basin in the SSTA, with values ranging from 1 to 2°C amplitude. The westward propagation of SHAA (Figure 7a) is evident for the Rossby-1 mode with 2 to 4 years scale variability. The small variability (amplitudes of the order of 1 cm) of the Rossby-2 mode is dominated by intra-annual events of about 1 to 2 months time scale with interannual variability superimposed. The SSTA space-time diagram (Figure 7b) shows that there is some indication of westward propagation at interannual time scales for the Rossby-1 mode, although higher frequency (time scale shorter than one month) variability masks the signal. For Rossby-2 mode, intra-annual and interannual are present but with amplitudes always smaller than 0.5°C. Using lag vs. longitude correlation diagrams of SHAA Rossby-1 coefficients (Figure 9, left), the westward phase velocity is estimated to range from 0.4 to 0.6 m/s. There is propagation of SSTA (Figure 9, right), but not as pronounced. The apparent continuity of SHAA Kelvin

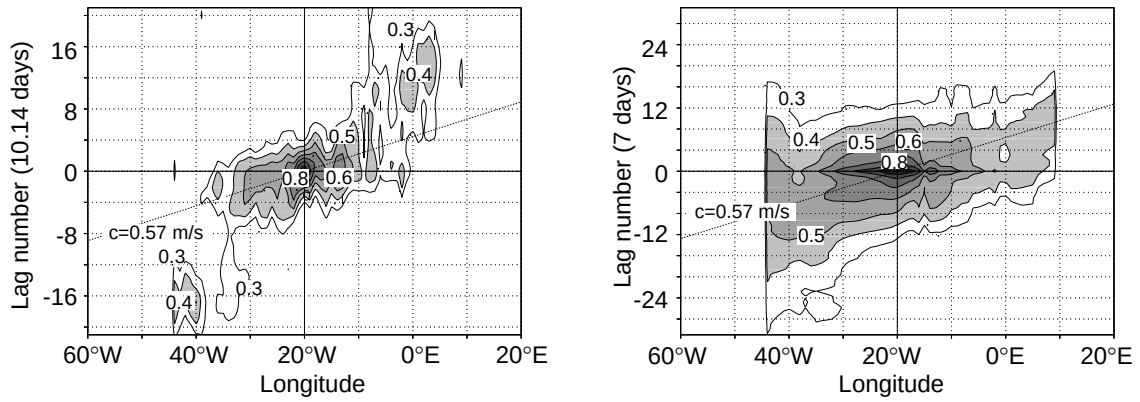

Figure 9. Lag vs. Longitude Correlation at 20^oW, for the Rossby-1 wave coefficient for (left) SHAA and (right) SSTA. Correlation significant at the 95% (99%) confidence limit is contoured (shaded).

and Rossby-1 coefficients close to the African coast is given by positive downwelling (negative upwelling) eastward propagating Kelvin coefficients which change to positive downwelling (negative upwelling) westward propagating Rossby-1 coefficients mainly at interannual periods (Figure 7a). This continuity is not as evident in the SSTA (Figure 7b).

Three longitudes are considered in the eastern, central and western Atlantic to test significant correlations among wave coefficients, The cross-correlation (ρ) at 40°W, 20°W and 0° (Greenwich meridian) between Kelvin and Rossby-1, and between Kelvin and Rossby-2 waves, of both SHAA and the SSTA, are shown in Figures 10a, 10b and 10c, and Figures 10d, 10e and 10f, respectively. The correlation function is shown for the time lag interval [-350,350] days. These correlation estimates have approximately 50 degrees of freedom, where values higher than 0.27 are significant at 95% confidence level and higher than 0.35 at 99%. Significant cross-correlation of SHAA, at the Greenwich meridian at 99% level is verified between Kelvin and Rossby-1 modes at time lags -30 to -50 days, with values greater than 0.45 reaching 0.50 at -40 days (Figure 10c). There is also significant negative cross-correlation, $\rho = -0.35$, between Kelvin and Rossby-2 modes at this longitude for 0 to 10 days time lag (Figure 10f). Along 20°W there is significant cross-correlation at lags 0 ($\rho = -0.57$) and -70 days ($\rho = 0.34$) between Kelvin and Rossby-1 (Figure 10b); and there is no significant cross-correlation at 20°W between Kelvin and Rossby-2 (Figure 10e). In the western portion of the tropical Atlantic there is no significant cross-correlations between the Kelvin and the two first meridionally trapped Rossby waves (Figures 10a and 10d) from SHAA data. Significant cross-correlation of the SSTA is verified only between the Kelvin and Rossby-2 waves at central and eastern longitudes around 0 time lag, values smaller

than -0.33 at time lags from -28 to -14 days at 20°W and $\rho = -0.30$ at zero lag at Greenwich meridian (Figures 10e and 10f). Significant cross-correlation between wave coefficients corresponding to different meridional modes around the zero lag may indicate locally generated anomalies projected over the modes. The significant cross-correlation between Kelvin and Rossby-1 modes at Greenwich (Figure 10c), lags -30 to -50 days, implies that a Kelvin wave leads the Rossby-1 wave by 30 to 50 days at this longitude, which is located approximately 10° off the meridional African coast. The phase velocity of the Rossby-1 mode, 1/3 of the Kelvin wave velocity, $c_{r1} = c_k/3$, is estimated to be between 1.0 m/s to 1.7 m/s. Considering the significant correlation at -70 days between Kelvin and Rossby-1 in the central basin, at 20°W, the phase velocity is estimated to be 2.0 m/s (Figure 10b).

The lagged cross-correlation between the Kelvin and Rossby-1 coefficients can also be seen as function of longitude in Figure 11 at 20°W for SHAA (left panel) and SSTA (right panel). Cross-correlation significant at the 99% confidence limit is shaded. The cross-correlation between Kelvin and Rossby-1 coefficients are significant at progressively higher negative lags as the longitudinal separation diminishes, indicating the westward progression of the Rossby-1 wave generated by the reflection of the Kelvin wave for SHAA (Figure 11, left). This feature is not as clear for SSTA (Figure 11, right).

5. DISCUSSION

Oceanic equatorial dynamic processes are important for understanding the influence of the ocean on the atmosphere and the interannual fluctuations in global weather patterns. Before altimetric data were used, the spatial and long period view of the variability in the tropical Atlantic was achieved using mostly SST data. However, the wave signal is masked in the SST measurement for two reasons: a) in the eastern basin, the shallow thermocline is associated with large SST variability and the consequent local radiative balance variability, which mask the thermal energy variation in the water column that may have a deeper origin; and b) in the western basin, the deeper thermocline leads to small SST changes which makes it difficult to identify the thermal energy variations or vertical movements of the thermocline. On the other hand, altimetry measures the sea height, a dynamically significant variable, and covers the total tropical Atlantic with a spatial resolution currently unrivaled by any other ocean measurement device for investigations of basin scale, long period, low signal to noise ratio ocean processes.

The accuracy and long period of T/P sampling allows to investigate the sea height signature of the equatorial waves, which have a very small magnitude in the tropical Atlantic, a region with lack of suitable sea height measurements and where the of the seasonal cycle is dominant. Two scales of interannual variability are present mainly associated with the sea surface temperature [*Servain et al.*, 1998]: one associated to the meridional dipole and with a predominant decadal scale [*Moura and Shukla*, 1981], and other to an El Niño-like, or Atlantic *Warm Event*, with a 2 to 4 years scale [*Merle*, 1980b; *Hisard*, 1980; *Carton and Huang*, 1994]. During the study period considered here (October, 1992 to May, 1999), coherent variability

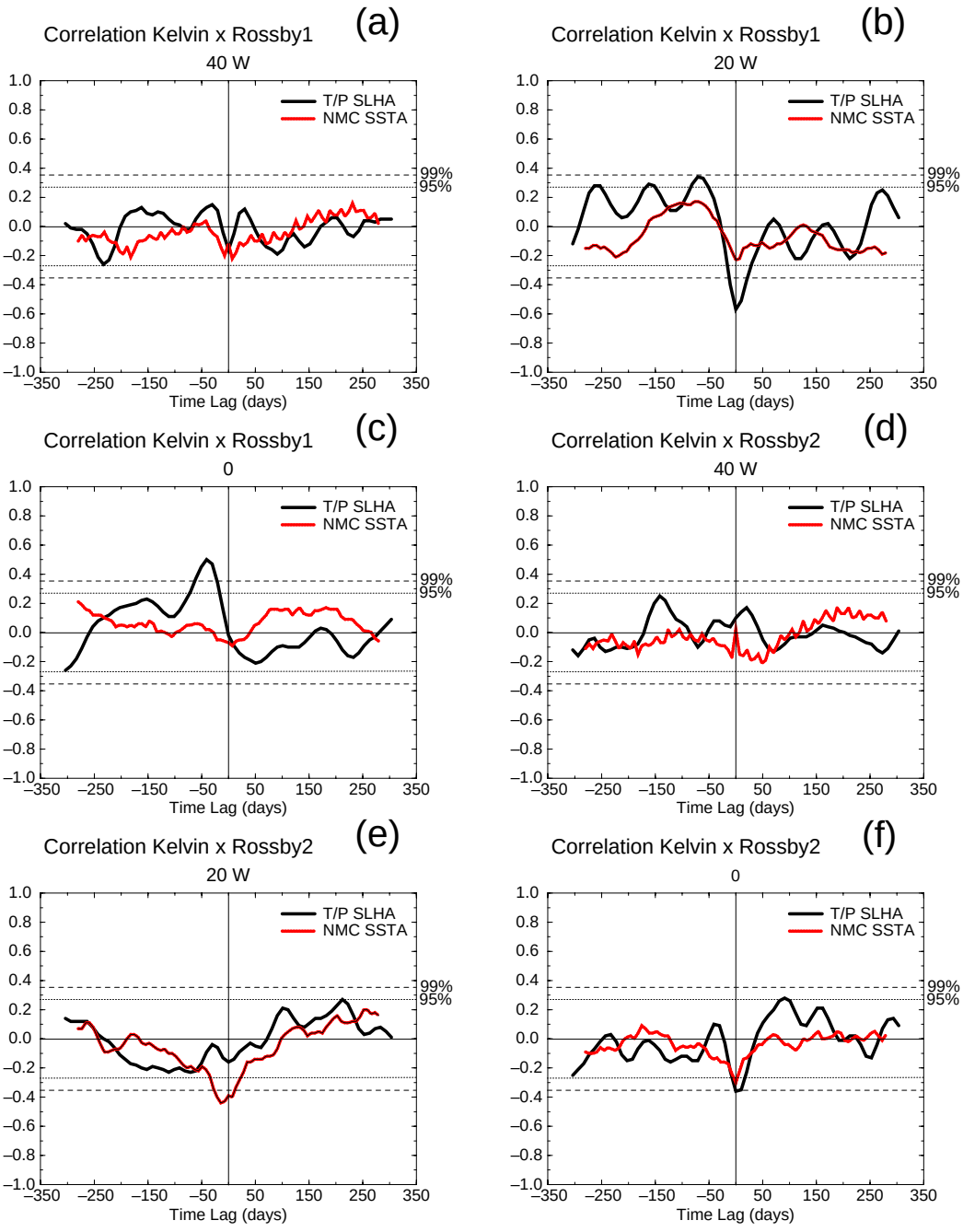

Figure 10. Cross-correlation between the coefficients h, estimated for T/P SHAA and SSTA, of the Kelvin wave and the first Rossby mode for (a) 40^oW (western basin), (b) 20^oW (central basin) and (c) 0^o Longitude (Greenwich Meridian, eastern basin) and the Kelvin wave and the second Rossby mode for (d) 40^oW (western basin), (e) 20^oW (central basin) and (f) 0^o Longitude (Greenwich Meridian, eastern basin).

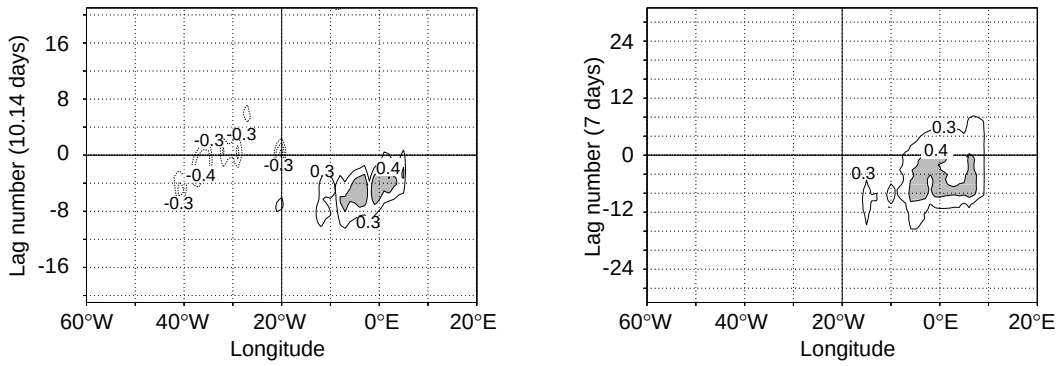

Figure 11. Lag vs Longitude Cross-correlation at 20^oW, between the Kelvin and Rossby-1 wave coefficients for (left) SHAA and (right) SSTA. Correlation significant at the 95% (99%) confidence limit is contoured (shaded).

is observed with 2 to 4 years period associated with the *Warm Events* and superimposed to the annual cycle.

As already indicated, the identification of planetary equatorial waves in the Atlantic is an important step to understand the equatorial dynamics. The number and the specific meridional modes, chosen as a subspace of the infinity set, were selected here to allow the solution of the system and the lowest modes; with 1° (or approximately 100 km) meridional resolution of the SHAA maps near the African and South American continents only 15 values are available to fit in the least square sense the wave coefficients. The lowest modes were chosen because dissipation is more efficient over higher modes, even though the linear equatorial long wave theory is inviscid [*Matsuno*, 1966]. The energy distribution between the modes (Figure 6) seems to show that the choice was adequate. The lowest modes dominate the variability of the SHAA and near the boundaries more modes present significant energy. However, virtually all energy is contained in the first 3 modes, with most energy in the first two modes, Kelvin and Rossby-1.

Kelvin wave coefficients propagate eastward and Rossby wave coefficients propagate westward as expected from linear theory. The velocities of propagation estimated for Kelvin and Rossby-1 modes, approximately 1.7 m/s and 0.6 m/s, are close to theoretical values for the first baroclinic mode [*Philander*, 1990]. From these waves coefficients it is noted that Kelvin and Rossby-1 waves are present in the T/P measurements of SHAA in the tropical Atlantic at interannual time scales.

The continuity of the Kelvin wave coefficients and Rossby-1 wave coefficients noticed in the deseasoned SHAA near the African coast is also predicted by linear equatorial wave reflection theory [*Moore and Philander*, 1976], where a Kelvin wave propagating eastward impinging in a meridional east tropical ocean coast would be reflected into symmetrical westward propagating Rossby waves and coastal Kelvin waves. It is expected from theoretical considerations that half of the incoming energy of the Kelvin wave be reflected as the first meridional Rossby mode for

long, non-dispersive wavelengths [*Clarke*, 1983]. Since the energy flux is conserved in the reflection and the Rossby-1 mode is three times slower than the Kelvin wave, the amplitude of the former should be higher than the later, as indicated in our estimates (Figure 6). On the other hand, the present analysis cannot reveal coastal waves. The reflection of Kelvin into Rossby waves implies a correlation between the waves at a lag that varies with the distance from the reflecting coast. Since the wave coefficients are orthogonal they should be statistically uncorrelated. Therefore, the presence of a statistically significant correlation at an appropriate lag between the wave coefficients obtained from SHAA shows wave reflection. The reflection of a equatorial Kelvin wave into a first meridional Rossby mode in the eastern Atlantic occurs in the African coast. Reflection in the western Atlantic is more difficult to detect because of the limitations imposed by the shape of North Brazilian coast and by the dispersive nature of the short wavelength Rossby modes.

The presence of Kelvin and Rossby waves in the SHAA data in the Atlantic at interannual time scales have dynamical implications. Two important mechanisms can be speculated: 1) a relaxation of the warm pool in the Western Atlantic similar to the mechanism proposed for the Pacific [*Wyrtki*, 1975], a pure oceanic mode; and 2) a coupled ocean-atmosphere mode, by which the waves are initially forced by instability in the atmosphere similar to the *delayed oscillator* theory. Although there is evidence of the first mechanism from observations of the sea surface temperature in the Gulf of Guinea and of the wind field in the Western Atlantic [*Servain et al.*, 1982], the second cannot be ruled out. The evidence of Kelvin and Rossby-1 waves mainly at eastern Atlantic corroborates the warm pool relaxation mechanism. Measurements of wind, sea temperature and sea height in key locations of the tropical Atlantic, such as the sites of the PIRATA moorings program [*Servain et al.*, 1998], combined with altimetry data will be very critical to fully understand the dynamical problem.

6. SUMMARY AND CONCLUSIONS

In the present work, deseasoned sea height anomalies from TOPEX/POSEIDON were used in the tropical Atlantic to investigate the presence of equatorial waves during 1992 to 1999. These anomalies were mapped into a regular $1^\circ \times 1^\circ$ grid using an Optimal Linear Interpolation scheme and then projected over the vectorial subspace spanned by the lowest meridional modes of the first baroclinic mode of the equatorial waves. It is shown that the first 3 waves (Kelvin and first two Rossby modes) explain virtually all the variance of the SHAA field in the tropical Atlantic, with the two first (Kelvin and Rossby-1) being predominant. Although the SHA variability is dominated by the seasonal cycle, the interannual and intra-annual scales are also present. The analysis presented here was centered in the deseasoned SHA, which is dominated by interannual variability with 2 to 4 year time scale, avoiding spurious serial correlations. The existence of the waves is strongly suggested by the velocities and directions of phase propagation, 1.7 m/s to the east for Kelvin waves and 0.6 m/s to the west for Rossby-1 waves, which agrees with the linear theory [*Matsuno*, 1966]. Moreover, a significant correlation is shown be-

tween Kelvin and Rossby-1 waves near the African coast at lags (50 days at the Greenwich meridian) that supports the idea of Kelvin wave reflection at the coast, agreeing with theoretical modeling [*Moore and Philander*, 1976].

Acknowledgments

We would like to thanks the CNES/AVISO system for providing altimetry data and the LCCA-USP (Laboratório de Computação Científica Avançada da Universidade de São Paulo) for the support. This work was partially supported by grants FAPESP-00/02958-7 and CNPq 300223/93-5, and by NOAA/AOML.

References

Arnault, S., and R. Cheney, Tropical Atlantic sea level variability from GEOSAT (1985-1989)., *J. Geophys. Res.*, *99*, 18,207–18,223, 1994.

Arnault, S., A. Morlière, J. Merle, and Y. Ménard, Low-frequency variability of the tropical Atlantic surface topography: Altimetry and model comparison., *J. Geophys. Res.*, *97*, 14,259–14,288, 1992.

AVISO, Aviso user handbook for merged TOPEX/POSEIDON., *Products. AVI-NT-02-101-CN, Edition 3.0* ., 1996.

Battisti, D., The dynamics and thermodynamics of a warming event in a coupled tropical atmosphere/ocean model., *J. Atmos. Sci.*, *45*, 2889–2919, 1988.

Boulanger, J.-P., and L.-L. Fu, Evidence of boundary reflection of Kelvin and first-mode Rossby waves from TOPEX/POSEIDON sea level data., *J. Geophys. Res.*, *101*, 16,361–16,371, 1996.

Boulanger, J.-P., and C. Menkes, Propagation and reflection of long equatorial waves in the Pacific ocean during 1992-1993 El Niño., *J. Geophys. Res.*, *100*, 25,041–25,059, 1995.

Boulanger, J.-P., and C. Menkes, Long equatorial wave reflection in the Pacific ocean from TOPEX/POSEIDON data during the 1992-1998 period., *Clim. Dyn.*, *15*, 205–225, 1999.

Busalacchi, A., and J. Picaut, Seasonal variability from a model of the tropical Atlantic ocean., *J. Phys. Oceanogr.*, *13*, 1564–1588, 1983.

Carton, J., and B. Huang, Warm events in the tropical Atlantic., *J. Phys. Oceanogr.*, *24*, 888–903, 1994.

Cartwright, D., and R. Tayler, New computations of the tide-generating potential., *Geophys. J. R. Astr. Soc.*, *23*, 45–74, 1971.

Chambers, D., B. Tapley, and R. Stewart, Long-period ocean heat storage rates and basin-scale heat fluxes from TOPEX., *J. Geophys. Res.*, *102*, 10,525–10,533, 1997.

Clarke, A., The reflection of equatorial waves from oceanic boundaries., *J. Phys. Oceanogr., 13*, 1193–1207, 1983.

Delcroix, T., J. Picaut, and G. Eldin, Equatorial Kelvin and Rossby waves evidenced in the Pacific ocean through GEOSAT sea level and surface current anomalies., *J. Geophys. Res., 96*, 3249–3262, 1991.

Delcroix, T., J.-P. Boulanger, F. Masia, and C. Menkes, Geosat-derived sea level and surface current anomalies in the equatorial Pacific during 1986-1989 El Niño and La Niña., *J. Geophys. Res., 99*, 25,093–25,107, 1994.

Delcroix, T., B. Dewitte, Y. duPenhoat, F. Masia, and J. Picaut, Equatorial waves and warm pool displacements during the 1992-1998 El Niño Southern Oscillation events: Observation and modeling., *J. Geophys. Res., 105*, 26,045–26,062, 2000.

duPenhoat, Y., and Y. Gouriou, Hindcasts of equatorial sea surface dynamic height in the Atlantic in 1982-1984., *J. Geophys. Res., 92*, 3729–3740, 1987.

França, C., I. Wainer, and A. Mesquita, A note on removing elastic ocean tide from TOPEX/POSEIDON data., *Int. J. Rem. Sens., 22*, 2927–2937, 2001.

Gill, A., and P. Niiler, The theory of the seasonal variability in the ocean., *Deep Sea Res., 20*, 141–177, 1973.

Gordon, A., Interocean exchange of thermocline water., *J. Geophys. Res., 91*, 5037–5046, 1986.

Gourdeau, L., J. Minster, and M. Gennero, Sea level anomalies in the tropical Atlantic from Geosat data assimilated in a linear model, 1986-1988., *J. Geophys. Res., 102*, 5583–5594, 1997.

Hastenrath, S., On meridional heat transports in world ocean., *J. Phys. Oceanogr., 12*, 922–927, 1982.

Hisard, P., Observation de réponses de type “El Niño” dans l’Atlantique tropical oriental Golfe de Guinée., *Oceanologica Acta, 3*, 209–220, 1980.

Katz, E., Equatorial Kelvin waves in the Atlantic., *J. Geophys. Res., 92*, 1894–1898, 1987.

Katz, E., Waves along the equator in the Atlantic., *J. Phys. Oceanogr., 27*, 2536–2544, 1997.

Knudsen, P., and O. Andersen, Sea surface temperature data (ATSR) vs. sea surface height data (T/P)., *AVISO Newsletter, 5*, 15–17, 1997.

Liebelt, P., *An introduction to optimal estimation.*, Addison Wesley, Reading, MA., 1967.

Matsuno, T., Quasi-geostrophic motions in the equatorial area., *J. Met. Soc. Japan*, *44*, 25–43, 1966.

Mayer, D., R. Molinari, M. Baringer, and G. Goni, Transition regions and their role in the relationship between sea surface height and subsurface temperature structure in the Atlantic ocean., *Geophys. Res. Lett.*, *28*, 3943–3946, 2001.

McCreary, J., J. Picaut, and D. Moore, Effects of remote annual forcing in the eastern tropical Atlantic ocean., *J. Mar. Res.*, *42*, 45–81, 1984.

Merle, J., Seasonal heat budget in the equatorial Atlantic ocean., *J. Phys. Oceanogr.*, *10*, 464–469, 1980a.

Merle, J., Variablité thermique annuelle et interannuelle de l'océan Atlantique équatorial est. l'hypothèse d'un "El Niño" Atlantique., *Oceanologica Acta*, *3*, 209–220, 1980b.

Merle, J., M. Fieux, and P. Hisard, Annual signal and interannual anomalies of sea surface temperature in the eastern equatorial Atlantic ocean., *Deep Sea Res.*, *26A*, 77–101, 1980.

Moore, D., and S. Philander, Modelling of the tropical oceanic circulation., in *The Sea*, vol. 6, pp. 319–361, Wiley, New York, 1976.

Moura, A., and J. Shukla, On the dynamics if droughts in northeast Brazil: observations, theory and numerical experiments with a general circulation model., *J. Atmos. Sci.*, *38*, 2653–2675, 1981.

Philander, S., *El Niño, La Niña and the Southern Oscillation.*, Academic Press, Inc., 1990.

Philander, S., and R. Pakanowski, A model of the seasonal cycle in the tropical Atlantic ocean., *J. Geophys. Res.*, *91*, 14,192–14,206, 1986.

Picaut, J., F. Masia, and Y. duPenhoat, An advective-reflective conceptual model for the oscillatory nature of the ENSO., *Science*, *277*, 663–666, 1997.

Priestley, M., *Spectral Analysis and Time Series*, Academic Press, London, 1981.

Reynolds, W., and T. Smith, Improved global sea surface temperature analyses., *J. Clim.*, *7*, 929–948, 1994.

Schopf, P., and M. Suarez, Vacillations in a coupled ocean-atmosphere model., *J. Atmos. Sci.*, *45*, 549–567, 1988.

Schott, F., and C. Boning, The WOCE model in the western equatorial Atlantic: Upper layer circulation., *J. Geophys. Res.*, *96*, 6993–7004, 1991.

Servain, J., Simple climatic indices for the tropical Atlantic ocean and some applications., *J. Geophys. Res.*, *96*, 15,137–15,146, 1991.

Servain, J., and J. Merle, *Interannual climate variations over the Tropical Atlantic Ocean.*, vol. 16 of *NATO ASI Series*, pp. 153–171, j. schukla ed., Springer-Verlag, Berlin Heidelberg, 1993.

Servain, J., J. Picaut, and J. Merle, Evidence of remote forcing in the equatorial Atlantic ocean., *J. Phys. Oceanogr.*, *12*, 457–463, 1982.

Servain, J., A. Busalacchi, M. McPhaden, A. Moura, G. Reverdin, M. Vianna, and S. Zebiak, A pilot research array in the tropical atlantic (PIRATA)., *Bull. Am. Meteorol. Soc.*, *79*, 2019–2031, 1998.

Servain, J., I. Wainer, J. McCreary, and A. Dessier, Relationship between the equatorial and meridional modes of climatic variability in the tropical Atlantic., *Geophys. Res. Lett.*, *26*, 485–488, 1999.

Shannon, L., A. Boyd, G. Brundrit, and J. Taunton-Clark, On the existence of an El Niño-type phenomenon in the Benguela system., *J. Mar. Res.*, *44*, 495–520, 1986.

Wagner, R., and A. da Silva, Surface conditions associated with anomalous rainfall in the Guinea coastal region., *Int. J. Climatol.*, *14*, 179–199, 1994.

Wahr, J., Deformation of the earth induced by polar motion., *J. Geophys. Res.*, *B90*, 9363–9368, 1985.

Wyrtki, K., El Niño-the dynamic response of the equatorial Pacific ocean to atmosphere forcing., *J. Phys. Oceanogr.*, *5*, 572–584, 1975.

Zebiak, S., Air-sea interaction in the equatorial Atlantic region., *J. Clim.*, *6*, 1567–1586, 1993.